Polymer Engineering & Science

WILEY | spe INSPIRING PLASTICS PROFESSIONALS

RESEARCH ARTICLE OPEN ACCESS

A Simplified Polymerization Model for Fluorinated Polymers: Average Microstructural Properties and Recipe Optimization

Luca Fois[1] | Daniela Bertani[2] | Matteo Fantoni[2] | Mattia Sponchioni[1] | Giuseppe Storti[1]

[1]Politecnico di Milano, Milano, Italy | [2]Syensqo S.A, Bollate, Italy

Correspondence: Mattia Sponchioni (mattia.sponchioni@polimi.it)

Received: 7 August 2025 | **Revised:** 14 October 2025 | **Accepted:** 14 October 2025

Funding: The authors received no specific funding for this work.

Keywords: average polymer properties | branching and pseudo living technology | fluorinated polymers | free radical emulsion polymerization

ABSTRACT

Fluoropolymers cover a wide range of industrial applications, due to their valuable mechanical and thermal properties. The microstructure of the final product is the key to controlling its end-use properties and to making them as close as possible to those required by the market. In this work, a model was proposed to evaluate the main average microstructural properties of the polymer, such as the number-average molecular weight and the number of the different chain ends per polymer chain, resulting from formulation parameters like the quantity of initiator, chain transfer agent, and crosslinking agent and corresponding addition policies. A representative kinetic scheme was proposed, involving an iodinated degenerative transfer agent and a crosslinking agent. The combination of these two additives allows tuning iodine incorporation within the chains, a key feature for the product post-processing. The model was first calibrated by fitting appropriate experimental data, then validated by exploiting additional data obtained under different operating conditions. Finally, the model was applied to determine the best feed policies for initiator, chain transfer agent and crosslinker ensuring the desired average properties of the final product. The reliability of the designed recipes was verified by comparison with experimental data obtained by implementing the addition policies predicted by the model.

1 | Introduction

Still today, fluoropolymers represent the materials of choice for applications in hostile environments due to their unique properties, such as remarkable resistance to chemicals, flame, and oxidative environments [1]. Among such materials, industrial sectors such as, chemical, aerospace, aircraft, petroleum, and energy often require the use of fluoroelastomers, due to their extraordinary sealing capabilities in corrosive and high-temperature environments [2].

The kinetics of the free radical polymerization of Tecnoflon, a vinylidene fluoride-hexafluoropropylene-tetrafluoroethylene (VDF-HFP-TFE) fluoroelastomer, is examined in this work. Using the so-called *branching and pseudo living technology* [3], that is in the presence of a pseudo-living agent (di-iodine transfer agent [4–8]) and a crosslinking agent (diolefin), a remarkable control of the polymer microstructure becomes possible. In particular, the incorporation of iodine at the chain ends is crucial for the post-processing of the latex obtained during an emulsion polymerization. On the other side, the diolefin favors the branching of the chain, with important implications in the mechanical properties of the fluoroelastomer. It turns out that a fine-tuning of the produced polymer microstructure is critical and affects the behavior of the rubber during post-processing, such as injection and compression molding, as well as the final mechanical properties of the cured item. Even though a detailed characterization of the polymer microstructure could be

Summary

- Emulsion polymerization model for a fluoroelastomer.
- Kinetic scheme with degenerative chain transfer agent and crosslinking agent.
- Recipe optimization to achieve target average microstructural properties.
- Addition policies designed to ensure homogeneous properties along the polymerization.
- Experimental validation of an optimized recipe suggested by the model.

performed by measuring the complete molecular weight distribution (MWD) as well as the branching and chain end group distributions, average values of the same properties are more often the available information at the industrial site and targets are set on these same average properties.

Therefore, starting from a comprehensive kinetic scheme of the reaction, a simplified model able to predict the main average microstructural properties, that is the number average molecular weight and the average number of different types of chain end groups per chain is developed in this work. The model was calibrated and validated using experimental data from pilot scale reactions, including polymerization rate and the mentioned average properties measured at different concentrations of initiator, chain transfer agent and crosslinker, and reactor pressure. Notably, in addition to evaluating the impact of the different additives on the polymer microstructure, the number of tetrafunctional branching points (or "bridges," BR) has been tracked, given the ability of such a feature to increase the number of iodinated chain ends per chain forming bridges between macromolecules.

After validation, the model was applied to design optimal addition policies of initiator, chain transfer and crosslinking agents aimed at controlling the polymer microstructure not only in terms of final values but, most importantly, in terms of consistency all along the reaction. Taking advantage of the model simplicity, analytical expressions of the addition rates could be obtained. The predicted addition laws was finally verified through specific experiments, confirming the model potential as a design tool for process optimization when the polymer quality is the primary requirement.

2 | Experimental Section

2.1 | Materials

The monomers, vinylidene fluoride ($CH_2 = CF_2$; purity 99.9%, gaseous), hexafluoropropylene ($CF_3CF = CF_2$; purity 99.9%, gaseous), and tetrafluoroethylene (C_2F_4; purity 99.9%, gaseous) have been used as produced by Syensqo, as well as the di-iodine transfer agent ($C_4F_8I_2$; purity > 99%, liquid)($C_4F_8I_2$; purity > 99%, liquid) and the diolefin ($CH_2CH(CF_2)_6CHCH_2$; purity 99.9%, liquid). The thermal initiator, ammonium persulfate ($(NH_4)_2S_2O_8$; purity 98.5%; Titolchimica) has been used as received. Deionized and demineralized water has been used as reaction medium.

2.2 | Reaction Conditions

All the reactions have been performed at 80°C and a constant pressure of 26 bar, with a single exception at 31 bar (run 6 in Table 1). In all cases, a constant composition terpolymer was produced, with VDF/HFP/TFE content equal to 70/20/10 mol%. A standard thermal initiator (ammonium persulfate, APS) was always used. Since enough latex stability is provided by the surface fixed charges introduced by the initiator fragments, the reactions could be run without emulsifier [9–14].

The recipes of all the experiments are reported in Table 1.

All the polymerizations have been carried out in a 10 L pilot plant reactor (Syensqo, Bollate, Italy) comprising a stainless-steel vessel equipped with two baffles and a stirrer. The stirring speed has been set to 545 rpm, large enough to ensure a chemical regime (negligible gas–liquid transport limitations [2]). A total of 5.6 L of water was used for each experiment reported in Table 1. The monomer mixture at the same composition as the desired terpolymer was continuously supplied to the reactor using a Hofer membrane pump, able to compress the gas up to a maximum of 40 bars, to maintain the reactor pressure constant and slowly enough to ensure fully starved conditions, that is minimal monomer accumulation in the reactor. This way, the resulting terpolymer is characterized by a constant composition all along the process and equal to that of the monomer mixture feed [15]. Indeed, all the reactions have been characterized by total instantaneous conversion during the entire process. Given the starved operating conditions and the negligible monomer solubility in water, the monomer feed flowrate is practically equal to the polymerization rate, thus becoming a very practical way of on-line conversion monitoring. The target mass of produced polymer was 2.5 kg in all the tests. As soon as this specific mass of monomer mixture was fed to the reactor, the reaction was quenched by rapid cooling. As shown in Table 1, the values of the actual mass of produced polymer slightly exceeded the target, due to the polymerization of the monomer mixture initially charged to pressurize the vessel. The temperature has been controlled through an external jacket in which water at 15°C or steam at 150°C has been used as cooling or heating fluid, respectively. The three monomers, stored separately, are subsequently mixed in the storage vessel at the desired composition in the gaseous state. Indeed, under the operating temperature and pressure, polymerization occured under supercritical conditions. A schematic representation of the setup employed in this work is shown in Figure 1.

Initiator and degenerative transfer agent (DTA) have been added as a single shot at the beginning of the reaction. For the diolefin, instead, a multi-shot (discretized additions) policy was employed. Each reaction was repeated multiple times and interrupted at different conversions, in order to provide the time evolution of the measured properties (conversion, number average molecular weight, M_n, and average number of different chain ends per unit mass of polymer). The results of the first three runs in Table 1 at increasing content of crosslinking agent have been used for model calibration. The validation experiments, runs 4 to 6, have been performed until complete conversion, thus providing only final values of the same properties. While run 5 has been carried out with the same addition policy of the calibration reactions, the addition of di-iodine

TABLE 1 | VDF/HFP/TFE terpolymerization recipes.

RUN	Final produced polymer [kg_{pol}]	Initiator concentration [g/kg_{pol}]	Degenerative transfer agent (DTA) [g/kg_{pol}]	Diolefin (DO) [g/kg_{pol}]	Pressure [bar]	Temperature [°C]	APS addition policy	DTA addition policy	DO addition policy
1	2.6[a]	1.6	4.6	—	26	80	Initial shot	Initial shot	Multi shot
2	2.6[a]	1.6	4.6	2.2	26	80	Initial shot	Initial shot	Multi shot
3	2.6[a]	1.6	4.6	3.6	26	80	Initial shot	Initial shot	Multi shot
4	2.6	0.5	9.2	3.8	26	80	Initial shot	Multi shot	Multi shot
5	2.6	0.8	4.6	2.2	26	80	Initial shot	Initial shot	Multi shot
6	2.7	0.9	6.9	4.6	31	80	Initial shot	Multi shot	Multi shot
7	2.6[a]	1.4	7.4	3.0	26	80	Initial shot	Initial shot	Multi shot
8	2.6[a]	1.4	7.4	3.0	26	80	Initial shot[b]	Cont. feed	Cont. feed

[a]Final value; multiple reactions carried out using the same recipe and quenched at intermediate conversion.
[b]50% of the total amount was added initially, with the rest added continuously.

agent has been performed using two more shots after the initial one for runs 4 and 6. The experimental values of the average polymer properties have been reported in this work normalized with respect to the final weight of produced terpolymer.

2.3 | Polymer Characterizations

The terpolymer microstructure has been evaluated in terms of average polymer properties.

The polymer molecular weight distribution (MWD) has been measured by gel permeation chromatography (GPC) equipped with a refractive index detector (Waters model 2414). The measurements were performed in anhydrous tetrahydrofuran (≥ 99.9%, 250 ppm BHT as inhibitor, Merck) at 35°C at a constant flowrate equal to 1 cm^3/min controlled by a dual-stroke piston pump (Waters; model 590). A set of four PLgel columns from Agilent with porosity 10^3, 10^4, 10^5, and 10^6 Å, have been used, respectively. The system was calibrated using polystyrene (PS) standards from Agilent. The MWD of branched polymers cannot be correctly evaluated through a single detector GPC; however, due to the very limited degree of long chain branching of the polymer under examination, this measurement was considered reliable enough [3]. The referred paper discusses a procedure for MWD evaluation validated considering fractionated and unfractionated samples and, as explained in Section 5, the reported results were considered significant and have been used in this study to quantify the contribution of diolefin to the formation of tetrafunctional branching points.

The average number of the different polymer chain end groups was measured by proton nuclear magnetic resonance (^{1}H NMR) spectroscopy (500 MHz), using Agilent DirectDrive System 500 operating at 499.86 MHz and acetone-d_6 (Merck; purity 99.9%) as solvent. The signal assignment and calculations on the NMR spectra have been performed following procedures already detailed in literature [16–18]. From these values, the average number of chain ends per macromolecule has been calculated through the ratio with the corresponding M_n. The final evaluation of experimental number average molecular weight has been performed through the universal calibration correction, as detailed in Section 1 of Supporting Information.

3 | Kinetic Scheme

The kinetic scheme sketched in Figure 2 was considered, where I_2 represents the thermal initiator in water phase, M monomer, DO and DTA the diolefin (*crosslinking* agent) and degenerative transfer agent (*living* agent), respectively, and M_{pol} the polymerized monomer. Note that in the figure each reaction is sketched twice, first specifying the chemistry of the species involved and then using the notation which will be adopted in the discussion of the model equations. These symbols will be explained in the following section (Model Development).

Even though three different monomers are involved, a simplified kinetic scheme has been exploited. Indeed, considering the more favored reactions based on mechanistic considerations

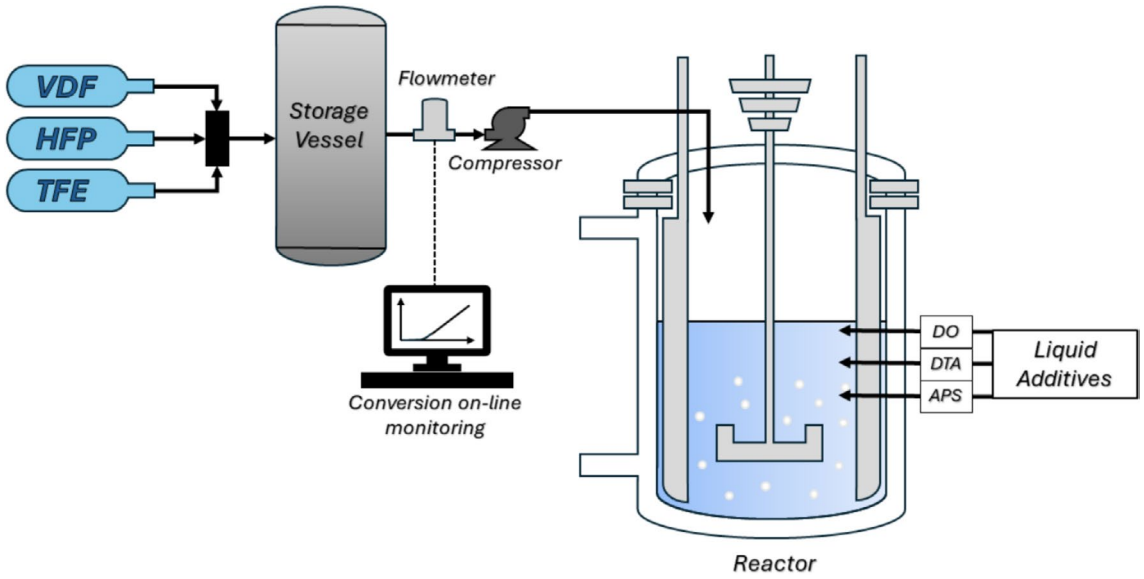

FIGURE 1 | Pilot plant scheme adopted for the emulsion polymerization of the terpolymer VDF/HFP/TFE.

[2], supported by the NMR analyses of main chain end types, the simplified, single-component kinetic scheme in Figure 2 has been used. Vinylidene fluoride has been selected as the representative monomer, i.e., the terminal unit of the active radical chains is more likely to derive from VDF than from the other comonomers, as confirmed by calculations reported in Section 2 of Supporting Information, where it emerges that the probability of having a terminal radical unit originated from VDF is >0.94, as supported by the reactivity ratios among the three monomers and the composition of the monomer feed. Based on this, reactions such as chain transfer to monomer, termination by disproportionation and chain transfer to polymer are based on the abstraction of hydrogen atoms from this species, involving in particular the $CF_2^{\bullet}$ radical type, which is the dominant one in these polymerization systems [2]. Accordingly, it should be emphasized that the estimated rate coefficients are only effective values, whose applicability is limited to the specific, constant terpolymer composition under examination.

Moreover, in Figure 2 the main chain end groups are also reported to identify the corresponding formation and consumption rates. Firstly, the hydroxide terminal group (CH_2OH) is generated in the radical formation reactions and, more specifically, by hydrolysis of the sulfur trioxide chain end group formed by propagation of the APS fragment with a monomer unit [19]. Then, the chain end groups generated by reactions involving the monomer are the methyl group (CH_3), from chain transfer to monomer, and fluorine hydrogenated groups (CF_2H) by chain transfer to polymer, backbiting and bimolecular termination by disproportionation, based on the considered kinetic scheme. On the other hand, terminal double bonds (TDB) are generated by chain transfer to monomer and bimolecular termination through hydrogen β-abstraction from the reacting radical [17].

As additional microstructural details, specific groups are shown useful to quantify the chain architecture. Namely, a mid-chain radical is formed by chain transfer to polymer, thus leading to the formation of a trifunctional branching point [20, 21] (BP). The same branching points are also formed by propagation to terminal double bond. In contrast to the short chain branching (SB) generated by the backbiting reaction, these trifunctional branching points form long chain branches along the chain.

The chain end groups formed by the reactions of the two main additives, di-iodine agent and diolefin, are also shown in the figure. Fluorine iodinated groups (CF_2I) are formed by degenerative transfer to the living agent. Notably, further transfer events do not change the overall number of fluorine iodinated groups incorporated in the polymer and, therefore, they are not relevant. On the other hand, the diolefin contributes to two different reactions: (i) the diolefin propagation reaction, in which a diolefin molecule (DO) reacts with a generic active chain, leading to the formation of a mid-chain group called pendant double bond (PDB); (ii) tetrafunctional branching points (BR) are formed by further propagation to the pendant double bond of a reacting radical chain.

Finally, the number of chains (C) and radical functionality (θ) are also tracked.

4 | Model Development

4.1 | Constitutive Equations

Given the simplified nature of the model, specific assumptions have been considered as summarized in the following.

1. As already mentioned, a pseudo-homopolymerization approach is applied [22], i.e., the copolymerization is described as a homopolymer considering a set of kinetic constants evaluated as composition-average of the values specific of each component. Since the terpolymer composition is constant during the reaction, these effective values are also constant [23].
2. The quasi-steady-state assumption (QSSA) has been used for radical species.

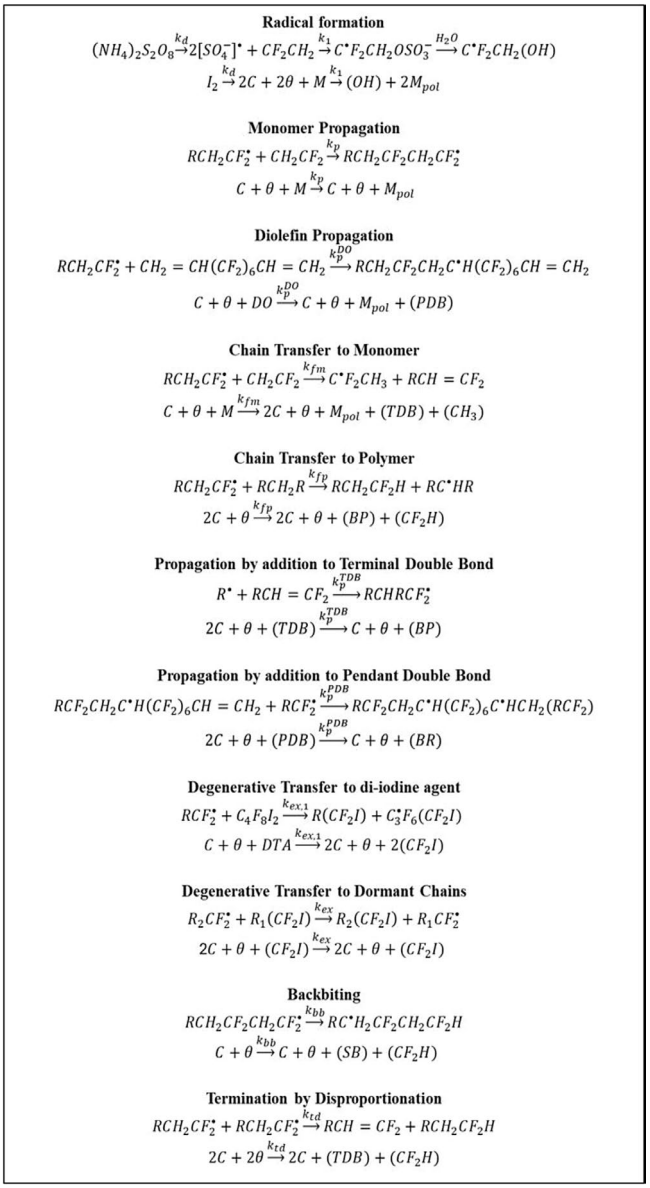

FIGURE 2 | Kinetic scheme considered in this work for the emulsion terpolymerization of VDF/HFP/TFE.

3. Chain length and property distributions are not accounted for, limiting the model outputs to average values such as average values of molecular weight and average number of chain end groups.
4. Pseudo-bulk conditions are considered, that is estimated values of the average number of radicals per particle resulted always larger than 0.5 [24] (cf. Section 3: Figure S1 of the Supporting Information): accordingly, the compartmentalized nature typical of the emulsion polymerization vanishes and the same equations typical of bulk polymerization can be used.
5. Monomer solubility in water has been neglected [25–27], due to the highly hydrophobic nature of all the monomers. Therefore, the particles become the dominant locus of the propagation reactions [28–30].
6. Vinylidene fluoride was selected as the representative monomer due to its predominant concentration in the three-component system and the marked prevalence of its corresponding radical species during the propagation stage.
7. Between the two possible propagation reactions typical of VDF, according to the quantum chemical simulations of Mavroudakis et al. [31], and to the results obtained in previous works [2, 32], the reactions forming head-type radicals occur much faster than those forming tail-type ones. For the system under evaluation, the probability of having head-type radicals is found to be larger than 90% and, therefore, only $CF_2^\bullet$ radical type has been considered as active species.
8. Semi-batch, constant pressure, perfectly stirred and isothermal reactor is assumed, also neglecting any monomer diffusion limitation [2].

According to the notation in Figure 2, the material balances have been written with reference not only to the species but also to the corresponding "properties." As an example, the polymer produced is expressed in terms of total number of chains, C, active, dormant and terminated, but an active chain brings also its radical end, indicated as θ. In this frame, N_C and N_θ are the corresponding total number of chains and active sites, respectively. This approach is especially effective to track the different chain-terminating and branching groups, the main focus of the model.

With reference to semi-batch, well-stirred and isothermal reactor with continuous addition of monomer and additives, the mass balances have been summarized in Table S4 of the Supporting Information using time as independent variable. Actually, the same equations can be conveniently reformulated using the extent of reaction (i.e., the number of moles of polymerized monomer, $N_{M_{pol}}$) as evolutionary variable. These equations are readily obtained by dividing each material balance by the overall polymerization rate and the resulting set of ordinary differential equations (ODEs) is shown in Table 2. The detailed derivation of Equation 1 from Equation S5 and S6 is reported in the Supporting Information, Section 4, as an example.

In these equations, the following notation has been used:

- N_x = overall number of moles of species x;
- y_x = ratio between the overall number of moles of species x and of polymerized monomer, $N_x / N_{M_{pol}}$;
- β_i = effective kinetic ratios, expressed as ratios between the rate constant of the i-th reaction and of propagation, k_i / k_p, with the exception of the initiator decomposition (all the ratios are defined in Table S5);
- $\widehat{q}_x$ = molar feed flowrate of species x specific to the number of moles of polymerized monomer, $\widetilde{q}_x / \frac{dN_{M_{pol}}}{dt}$.

The model is finally complemented by the following auxiliary algebraic equations:

- Monomer concentration in particle phase—According to the assumption of phase equilibrium inside the reactor, the monomer concentration in the particles at equilibrium has been evaluated through the Henry law, $C_M = HP$, where P denotes the total pressure. Given

TABLE 2 | Material balances with reaction extent, $N_{M_{pol}}$, as evolutionary variable.

Initiator	$\frac{dN_{I_2}}{dN_{M_{pol}}} = -\beta_{I_2}\frac{\sqrt{y_{I_2}MW_M}}{\sqrt{f\rho_{pol}}y_M} + \hat{q}_{I_2}$	(1)
Degenerative transfer agent	$\frac{dN_{DTA}}{dN_{M_{pol}}} = -\frac{2}{y_M}\beta_{DTA}y_{DTA} + \hat{q}_{DTA}$	(2)
Diolefin	$\frac{dN_{DO}}{dN_{M_{pol}}} = -\frac{2}{y_M}\beta_{DO}y_{DO} + \hat{q}_{DO}$	(3)
Polymer chain	$\frac{dN_C}{dN_{M_{pol}}} = 2f\beta_{I_2}\frac{\sqrt{y_{I_2}MW_M}}{\sqrt{f\rho_{pol}}y_M} + \frac{2}{y_M}\beta_{DTA}y_{DTA} + \beta_{fm} - \frac{1}{y_M}\beta_{TDB}y_{TDB} - \frac{1}{y_M}\beta_{PDB}y_{PDB}$	(4)
OH-end group	$\frac{dN_{OH}}{dN_{M_{pol}}} = 2f\beta_{I_2}\frac{\sqrt{y_{I_2}MW_M}}{\sqrt{f\rho_{pol}}y_M}$	(5)
CF_2H-end group	$\frac{dN_{CF_2H}}{dN_{M_{pol}}} = \frac{1}{y_M}\beta_{fp} + \frac{MW_M}{y_M\rho_{pol}}\beta_{bb} + \frac{\sqrt{fy_{I_2}MW_M}}{\sqrt{\rho_{pol}}y_M}\beta_{I_2}$	(6)
CH_3-end group	$\frac{dN_{CH_3}}{dN_{M_{pol}}} = \beta_{fm}$	(7)
CF_2I-end group	$\frac{dN_{CF_2I}}{dN_{M_{pol}}} = 2\left(\frac{2}{y_M}\beta_{DTA}\right)y_{DT}$	(8)
Terminal double bond	$\frac{dN_{TDB}}{dN_{M_{pol}}} = \beta_{fm} + \frac{\sqrt{fy_{I_2}MW_M}}{\sqrt{\rho_{pol}}y_M}\beta_{I_2} - \frac{1}{y_M}\beta_{TDB}y_{TDB}$	(9)
Trifunctional point (branching)	$\frac{dN_{BP}}{dN_{M_{pol}}} = \frac{1}{y_M}\beta_{TDB}y_{TDB} + \frac{1}{y_M}\beta_{fp}$	(10)
Short branch	$\frac{dN_{SB}}{dN_{M_{pol}}} = \frac{MW_M}{y_M\rho_{pol}}\beta_{bb}$	(11)
Pendant double bond	$\frac{dN_{PDB}}{dN_{M_{pol}}} = \frac{2}{y_M}\beta_{DO}y_{DO} - \frac{1}{y_M}\beta_{PDB}y_{PDB}$	(12)
Tetrafunctional point (bridge)	$\frac{dN_{BR}}{dN_{M_{pol}}} = \frac{1}{y_M}\beta_{PDB}y_{PDB}$	(13)

the multicomponent nature of the system, the constant H has been estimated as the average of the single component values as $H = \sum_{i=1}^{N_{mon}} x_i H_i$ [33], being x_i the mole fraction of the i-th monomer in the gas mixture. Neglecting the monomer solubility in water, the overall number of moles of monomer has been evaluated as:

TABLE 3 | Kinetic model parameters.

Parameter	Numerical value	95% confidence interval	Units	Source
k_d	1.08×10^{-3}	—	$[s^{-1}]$	[34]
k_p	2.10×10^{3}	—	$[L\,mol^{-1}\,s^{-1}]$	[2]
$k_{ex,1}$	$= k_p$	—	$[L\,mol^{-1}\,s^{-1}]$	[2]
k_{fp}	$2.8\times10^{-5}\,k_p$	—	$[L\,mol^{-1}\,s^{-1}]$	[2]
k_{td}	$25.7\,k_p$	—	$[L\,mol^{-1}\,s^{-1}]$	[2]
k_p^{DO}	$= k_p$	—	$[L\,mol^{-1}\,s^{-1}]$	This work
k_p^{TDB}	$8.6\times10^{-2}\,k_p$	$[4.7\times10^{-2}\div1.2\times10^{-1}]\,k_p$	$[L\,mol^{-1}\,s^{-1}]$	This work
k_p^{PDB}	$6.9\times10^{-3}\,k_p$	$[1.7\times10^{-3}\div1.2\times10^{-2}]\,k_p$	$[L\,mol^{-1}\,s^{-1}]$	This work
k_{fm}	$1.6\times10^{-4}\,k_p$	$[1.2\times10^{-4}\div1.9\times10^{-4}]\,k_p$	$[L\,mol^{-1}\,s^{-1}]$	This work
k_{bb}	$3.6\times10^{-4}\,k_p$	$[7.0\times10^{-5}\div6.5\times10^{-4}]\,k_p$	$[s^{-1}]$	This work

$$N_M = C_M V_p = HP\,V_p \tag{14}$$

where the volume of the particles is given by:

$$V_p = MW_M\left(\frac{N_{M_{pol}}}{\rho_{pol}} + \frac{N_M}{\rho_M}\right) \tag{15}$$

with MW_M average molecular weight representative of the monomer mixture and ρ_M and ρ_{pol} density of monomer mixture and polymer, respectively.

- Active chains in particle phase—The radical chains (active sites) can be estimated from the molar balance on N_θ imposing the quasi steady state assumption:

$$N_\theta = \sqrt{\frac{f k_d N_{I_2} V_p}{k_{td}}} \tag{16}$$

where k_d represents the initiator thermal decomposition rate constant, f the radical efficiency [34] and k_{td} the rate constant of bimolecular termination by disproportionation.

It is worth noting that DTA does not influence the number of active sites, since radical desorption as well as the retardation effect are expected to be negligible.

The numerical solution of Equations (1–16) provides the evolution of all the unknowns as a function of $N_{M_{pol}}$; if the time profiles are desired, the relationship between the number of moles of polymerized monomer and time is readily evaluated by integration of the corresponding material balance (Equation (S5) in Table S4).

Only the values of three out of eight effective kinetic ratios have been found in the literature, (specifically β_{I_2}, β_{DTA}, β_{fp}). The remaining five ratios have been estimated as follows:

- Given the similar chemical nature, the diolefin propagation rate constant has been assumed equal to monomer propagation, therefore $\beta_{DO} = 1$;
- The four other parameters (specifically β_{TDB}, β_{PDB}, β_{fm}, and β_{bb}) have been estimated by fitting the model predictions to experimental results. Namely, an optimization approach has been used based on hybrid genetic algorithm, obtained combining the function `ga` with the hybrid function `fmincon` in MATLAB.

4.2 | Control Problem: Target Properties and Optimal Flowrates

To design the operating conditions required to ensure the desired values of selected average properties as well as their consistency along the reaction, the model equations are now further worked out.

The model in Table 2 is made of 13 ODEs along with three algebraic Equations (14–16); the corresponding unknowns are 19 (15 overall number of moles of each species/property N_x, the particle volume V_p and three specific molar flowrates, $\hat{q}_{I_2}$, $\hat{q}_{DTA}$, and $\hat{q}_{DO}$). Then, three degrees of freedom remain, and they have been saturated by setting the desired polymer quality. Three target properties are identified and required to remain constant all along the polymerization, namely the number average degree of polymerization, DP_n, the average number of iodinated end groups per chain, and the average number of bridges per chain. The latter two properties have been selected because of their impact on the polymer quality: the iodinated groups represent the preferential sites of crosslinking by oxidative reactions during post-processing, while the tetrafunctional branching points impact the mechanical properties of the final product. Note that these two properties are interconnected, being the average number of iodinated end groups per chain affected by the extent of crosslinking, that is by the number of bridges per chain.

All the three selected properties can be conveniently quantified in terms of corresponding y_x values. Namely:

- Number average degree of polymerization

$$DP_n = \frac{N_{M_{pol}}}{N_C} = \frac{1}{y_C} \tag{17}$$

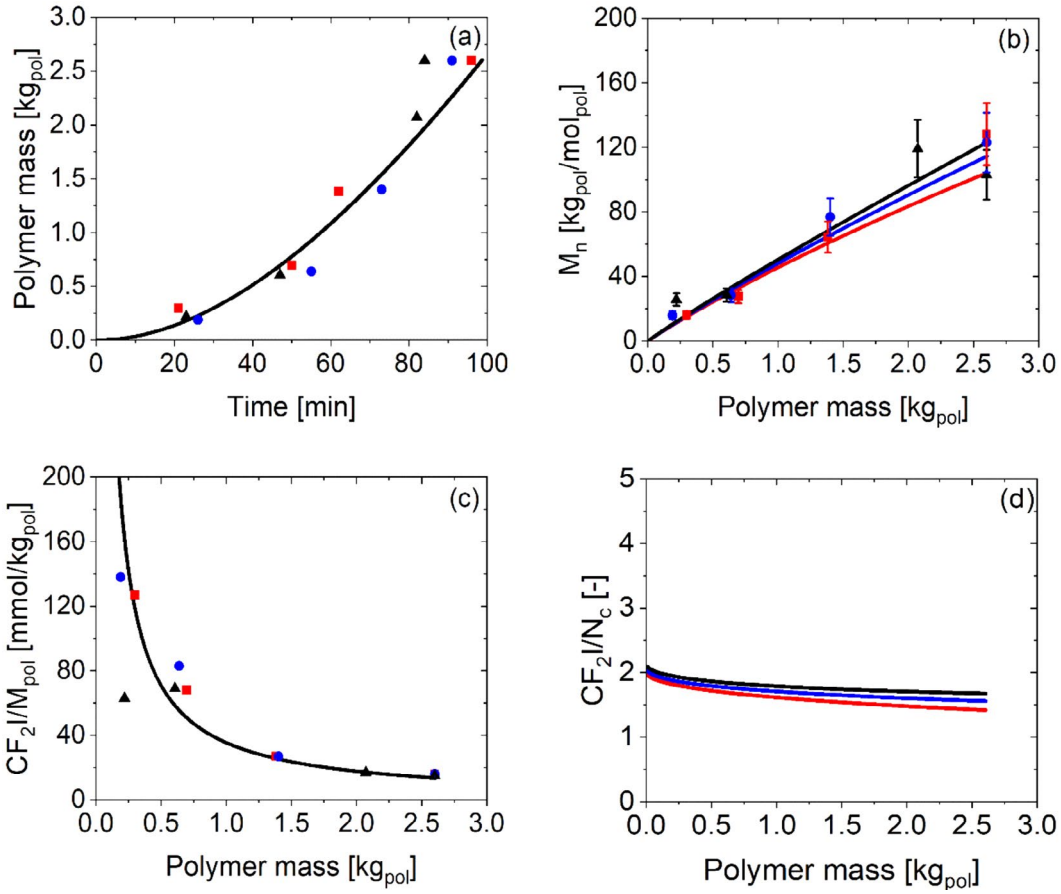

FIGURE 3 | (a) Produced polymer mass as a function of time, (b) Number average molecular weight, (c) CF_2I chain end groups per mass of polymer, (d) CF_2I chain end groups per chain. Experimental data: run 1 = red squares, run 2 = blue circles, run 3 = black triangles. Continuous curves: model results, same color as the corresponding experimental data. In (a) and (c) red and blue curves are overlapped to the black one and hence not visible.

– Average number of iodinated chain end groups per chain

$$\frac{N_{CF_2I}}{N_C} = \frac{y_{CF_2I}}{y_C} \tag{18}$$

– Average number of tetrafunctional branching points per chain

$$\frac{N_{BR}}{N_C} = \frac{y_{BR}}{y_C} \tag{19}$$

In order to ensure constant values of all these properties throughout the entire polymerization, the corresponding y values should also stay constant, a constraint which is fulfilled providing that:

$$d\left(\frac{N_x}{N_{M_{pol}}}\right) = 0 \text{ that is } \frac{dN_x}{dN_{M_{pol}}} = \frac{N_x}{N_{M_{pol}}} \equiv y_x \tag{20}$$

Given the general form of the material balances in Table 2, the latter equation reduces to:

$$y_x = -\frac{\mathcal{R}_x}{\mathcal{R}_{M_{pol}}} + \hat{q}_x \tag{21}$$

thus providing an explicit relationship between the value of the required property y_x, the reaction terms and the specific feed flowrates $\hat{q}_x$. Accordingly, given target values of the selected average properties and the corresponding y values through Equations (17–19), the optimal feed flowrates are readily evaluated using Equation (21) with $x = I_2$, DTA, and DO.

5 | Results

5.1 | Model Calibration

The calibration of the model has been performed by exploiting three sets of experimental data, each one obtained from repeated reactions stopped at different conversions, so as to track the variables of interest as a function of the reaction coordinate. This approach was adopted owing to the impossibility of performing reliable and safe sampling of the latex from the reactor while at high temperatures and pressures of fluorinated monomers. Considering both the technical limitations of the facility and the applicable safety and prevention regulations, online sampling of the reaction mixture was therefore deemed unfeasible.

The model calibration has been performed using some parameter values from the literature and evaluating the remaining ones by fitting the experimental data, as already mentioned in Section 4.

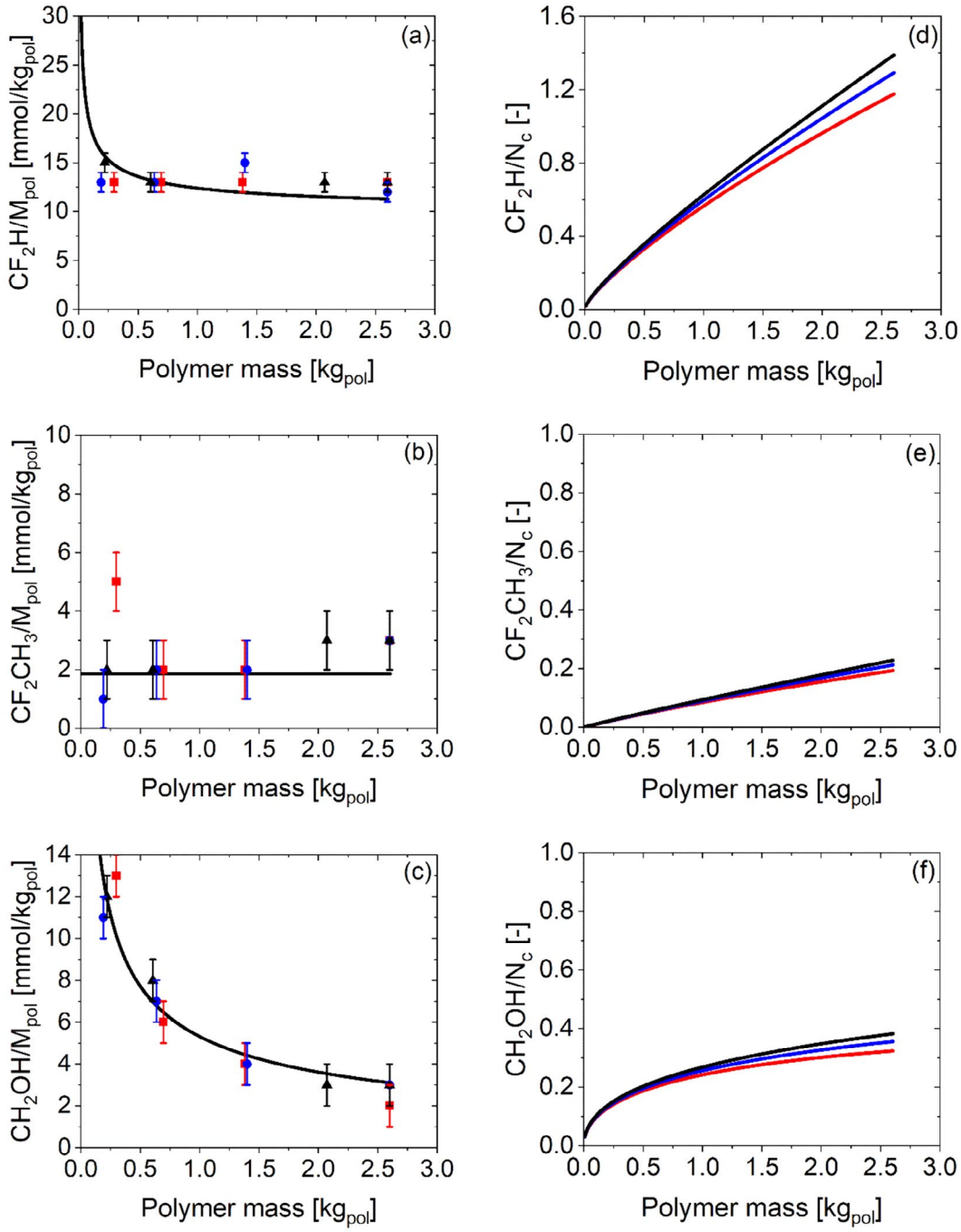

FIGURE 4 | (a) CF_2H chain end groups per mass of polymer, (b) CF_2CH_3 chain end groups per mass of polymer, (c) CF_2OH chain end groups per mass of polymer, (d) CF_2H chain end groups per polymer chain, (e) CF_2CH_3 chain end groups per polymer chain, (f) CF_2OH chain end groups per polymer chain as a function of produced polymer mass. Experimental data: run 1 = red squares, run 2 = blue circles, run 3 = black triangles. Continuous curves: model results, same color as the corresponding experimental data. In (a–c) red and blue curves are overlapped with the black ones and hence not visible.

The final values of the parameters involved in the model are reported in Table 3, with most of the pseudo-kinetic rate constants set equal to the values reported by Apostolo et al. [2, 35].

Using this set of rate constants, the model simulations for the calibration experiments (runs 1–3 in Table 1) are compared with the measured properties. Specifically, in Figure 3a, experimental data of produced polymer mass vs. time are reported. Due to the negligible contribution of the diolefin to the polymerization rate, the three curves calculated by the model are practically superimposed. Keeping in mind that each value is the result of a different experiment, the agreement between model and experiments is quite good. Moving on to the average properties, the main focus of the work, the values of number average molecular weight, $M_n = DP_n \cdot MW_M$, are shown in Figure 3b. As expected, higher diolefin contents lead to an increase in M_n because of the formation of crosslinking among the chains. However, such effect is quite weak because of the small amount of diolefin used in all cases together with the branching mitigation associated with the degenerative di-iodine transfer agent.

The iodine content in the polymer, expressed as number of CF_2I chain end groups per mass of polymer, is shown in Figure 3c: as expected, the three model curves are fully overlapped due to the identical content of di-iodine transfer agent in the three examined recipes. It is worth noting that the experimental values of incorporated iodine indicated a lack of iodine relative to the nominal amounts specified in Table 1. Across all the runs, the average value of such discrepancies is 29.57% ± 2.9%: therefore, a constant iodine loss of 30% was assumed for all the simulations. This loss reflects the known effect of thermal initiation on iodofluorocarbon compounds, which degrade free iodine leaving inert species no longer able to contribute to the degenerative transfer reactions [7, 36]. The selected value of the percentage loss was estimated using a large set of experimental data collected by the industrial partner and represents a reliable estimate.

Together with M_n and iodine chain ends, the model can be exploited to track other end groups coming from the initiator or from the specific radical termination. In Figure 4a, experimental data for runs 1, 2, and 3 of CF_2H per mass of produced polymer has been reported. These data were particularly useful for the estimation of the backbiting kinetic rate constant, since the other kinetic parameters involved in the formation of these specific groups have been selected by literature. In Figure 4b, both the experimental and model results for CF_2CH_3 chain end groups are reported. This chain end group is only related to chain transfer to monomer reaction, according to the kinetic scheme considered in this work. Finally, the CF_2OH chain end group per mass of polymer has been tracked during time to verify the consistency of the initiator decomposition rate constant k_d, as reported in Figure 4c. In Figure 4d,e, the same end groups are reported as average values per polymer chain for completeness.

The propagation to pendant double bond rate constant k_p^{PDB} has been evaluated by taking advantage of the experimental number of tetrafunctional branching points reported in the literature to be equal to 0.1 [3]. Since the terpolymers analyzed in the referred article are the same studied in this work (same composition and similar contents of di-iodine agent and diolefin), this experimental value has been considered meaningful. It is worth highlighting that the work by Maccone et al. [3] was carried out under microemulsion polymerization conditions and was modeled by Apostolo et al. [35] using a segregated approach. To exploit this experimental dataset consistently, a modified model accounting for radical segregation was employed, as detailed in Section 4 of the Supporting Information. As a result of the optimization process, the model was able to accurately reproduce the final BR / N_C content.

5.2 | Model Validation

After model calibration, its validity was demonstrated by predicting the evolution of three additional experiments (Table 1,

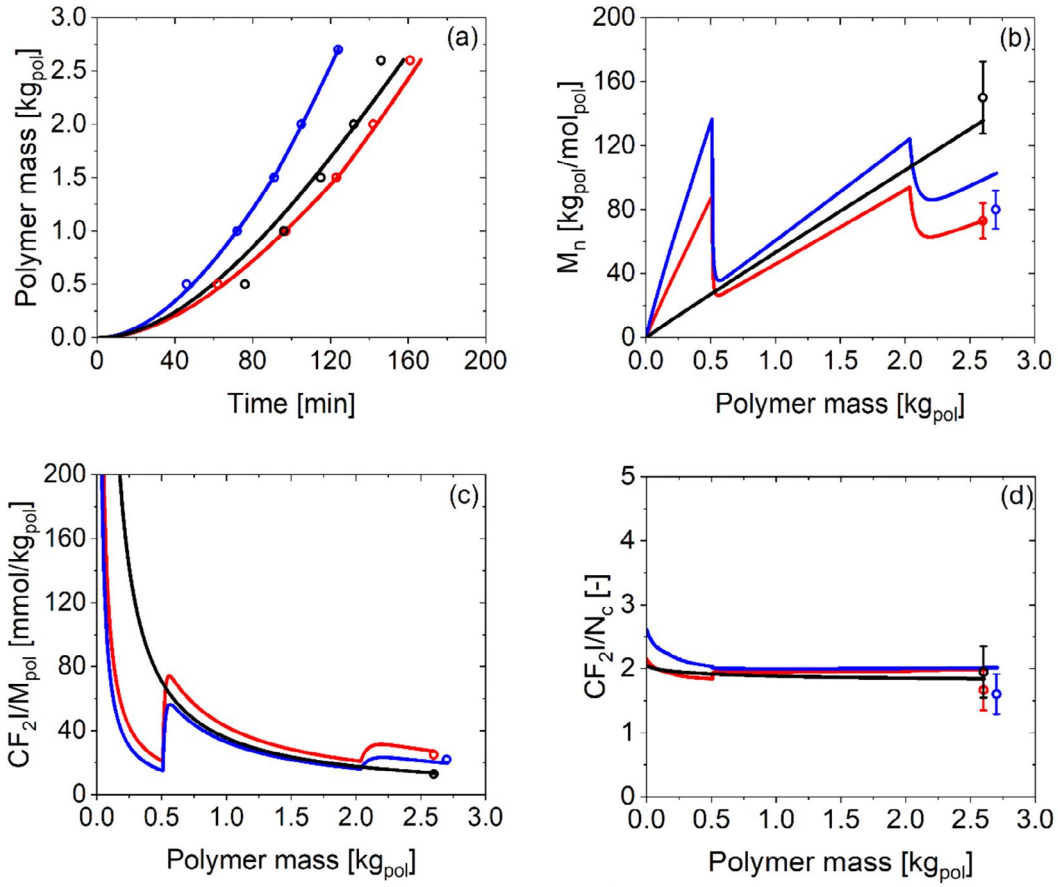

FIGURE 5 | (a) Produced polymer mass as a function of time, (b) Number average molecular weight, (c) CF_2I chain end groups per mass of polymer, (d) CF_2I chain end groups per chain as a function of produced polymer mass. Experimental data: run 4 = red circles, run 5 = black circles, run 6 = blue circles. Continuous curves: model results, same color as the corresponding experimental data.

runs 4, 5, and 6). Since only final values of the average properties are experimentally available in this case, the comparison with the model predictions is carried out for the entire time evolution only for the produced polymer mass. Moreover, given the validation nature of this comparison, the parameter values estimated in the previous section have been used without modification, that is in a genuinely predictive mode.

The reaction kinetics are shown in Figure 5a for all the reactions and the agreement between the model and experiments is quite good in all cases. The prediction is equally good for the average properties, even though final values were only available. The calculated evolutions of number average molecular weight are reported in Figure 5b, where the profiles are consistent with the additions of degenerative transfer agent. For runs 4 and 6, after the initial injection, the di-iodine agent has been further added at two intermediate conversions. Such shots generate an instantaneous decrease in average molecular weight due to the sudden increase in the number of chains. On the other hand, DTA was only initially injected in run 5 where, in fact, the regular, linear increase in molecular weight, typical of living polymerization reactions, is found.

In Figure 5c,d, the predicted profiles of iodinated chain end groups CF_2I per mass of polymer and per chain, respectively, are reported. The agreement with the final experimental values is still good and, once more, the discretized addition policy of the DTA results in an almost instantaneous increase in the incorporated iodine.

Similarly good agreement between model and experiments has been verified for other average properties, namely CF_2H, CF_2CH_3, and CH_2OH end groups. Such comparisons are shown in Figure S2. Overall, these results provide a convincing validation of the reliability of the estimated parameter values, thus supporting the use of the model to explore different recipes and feed policies.

5.3 | Optimal Feed Flowrates

To evaluate the potential of the proposed model in the development of reaction recipes allowing a fine tuning of the polymer quality, an applicative example was considered by targeting the following values of the properties of interest:

$$M_n = 75\ \mathrm{kg/mol} \qquad CF_2I/N_C = 1.8 \qquad BR/N_C = 0.07$$

This set of values characterizes a product with suitable microstructural properties, including a moderate molecular weight, an appropriate number of iodine atoms per chain to enable effective post-polymerization crosslinking, and a limited number of branching points per chain. The latter ensures that the final material remains processable. Not only was the target placed on the values of these properties, but the aim was also preserving their consistency all along the reaction. From these constraints, the corresponding optimal flowrates are readily calculated through Equations (22–24), obtained by taking advantage of Equation (21):

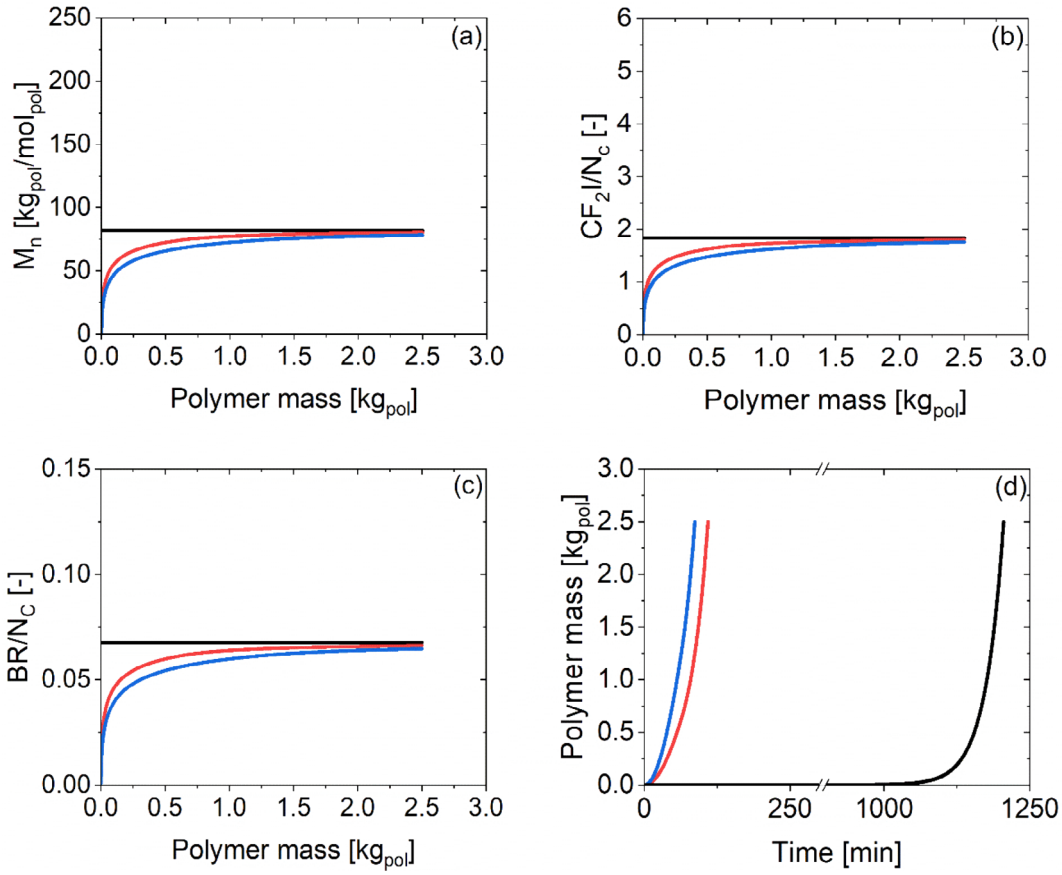

FIGURE 6 | Calculated values of (a) Number average molecular weight, (b) CF_2I chain end groups per mass of polymer, and (c) BR chain end groups per chain as a function of produced polymer mass. (d) Calculated conversion vs. time. Black curve = optimal feed flowrates; red and blue curves = initial APS shot equal to 25% and 50%, respectively.

$$\hat{q}_{I_2} = y_{I_2} + \beta_{I_2} \frac{\sqrt{y_{I_2} MW_M}}{\sqrt{f \rho_p} y_M} \tag{22}$$

$$\hat{q}_{DTA} = y_{DTA} \left(1 + \frac{2}{y_M} \beta_{DTA} \right) \tag{23}$$

$$\hat{q}_{DO} = y_{DO} \left(1 + \frac{2}{y_M} \beta_{DO} \right) \tag{24}$$

These relationships provide the constant $\hat{q}_x$ values suitable to ensure consistent value of the corresponding y_x equal to the setpoint. The detailed expressions linking the specific molar flow rates of the operating variables to the target values y_k^* (with $k = C$ (i. e., M_n), CF_2I, BR) are provided in Section 6 of the Supporting Information.

The model-predicted flowrates corresponding to the selected target properties listed above are as follows.

$$\hat{q}_{I_2} = 5.02 \times 10^{-4} \left[\frac{\text{mol}_{I_2}}{\text{mol}_{\text{pol}}} \right]$$

$$\hat{q}_{DTA} = 1.10 \times 10^{-3} \left[\frac{\text{mol}_{\text{DTA}}}{\text{mol}_{\text{pol}}} \right]$$

$$\hat{q}_{DO} = 7.14 \times 10^{-4} \left[\frac{\text{mol}_{\text{DO}}}{\text{mol}_{\text{pol}}} \right]$$

Using these flowrates, the resulting polymer quality is then evaluated in Figure 6a–c (black lines). As expected, the target values of the three properties are achieved from the beginning of the reaction, and preserved until the end, thus ensuring fully homogeneous product. However, the reaction rate, as shown in Figure 6d (black curve) is definitely too low, with final conversion reached only after more than 1 day of reaction. This too long reaction duration comes from the implemented feed flowrate of initiator: using this flowrate, the desired average chain length is indeed maintained from the beginning but at the expenses of such a small radical concentration that negligible polymerization rates are obtained for most of the reaction.

Therefore, to overcome this limitation, an effective strategy we adopted was to modify the initiator addition policy by adding a given fraction of the predicted cumulative amount of APS at the beginning of the polymerization and the remainder using the predicted optimal flowrate. The time at which the feed is started is simply evaluated as the time at which the APS fraction initially assumed would be cumulatively fed using the optimal flowrate. This empirical modification of the calculated feed policy is expected to accelerate the reaction, thus reducing the reaction time. On the other hand, this may also impact the homogeneity of the polymer quality. To verify its impact, in Figure 6 we simulated two different initial shots of initiator, namely 25% (red curves) and 50% (blue curves) of the cumulative amount. Following this initial shot, a significant acceleration of the reaction can be observed (Figure 6d) at the expenses of an initial discrepancy between target and actual properties in all cases (Figure 6a–c). Such discrepancy is negligible in terms of final, cumulative property (all curves converge to the same plateau value equal to the target) but reveal some heterogeneity with respect to the optimal, fully homogeneous case. To quantify such heterogeneity, the parameter $H(y)$ has been calculated for each property y as:

$$H(y) = \frac{\int_0^{N^f_{M_{pol}}} y \, dN_{M_{pol}}}{y_{opt} N^f_{M_{pol}}} \times 100 \tag{25}$$

where $N^f_{M_{pol}}$ is the final value of moles of polymerized monomer and y_{opt} the target value of the same property. The resulting values are 5% and 9% when the initial fraction of APS is 25% and 50%, respectively, whatever is the examined property: therefore, a limited extent of heterogeneity is introduced in all cases.

To conclude, the optimal feed flowrates are proved fully effective in producing the desired polymer quality with perfect homogeneity. On the other hand, the issue of too long reaction time is easily handled by the initial injection of a fraction of the predicted initiator amount while the remaining initiator is later fed according to the predicted optimal law. This enables much shorter reaction time, although at the expenses of a slight heterogeneity of the polymer.

5.4 | Addition Policies: Constant Properties (CP) vs. Pseudo-Living (PL)

The first three experimental runs in Table 1 were carried out according to the previously mentioned *branching and pseudo living technology*, with initial addition of iodinated agent and initiator and distributed addition of the crosslinking agent. Accordingly, as typical of living reactions, the number average molecular weight increases almost linearly with conversion, while all the chain end groups monotonically decrease. Therefore, even though the final properties exhibit the target values, these are not constant with the reaction extent. In contrast, the optimal feed flowrates proposed above ensure these same values of the average properties all along the reaction.

To illustrate these considerations, two comparative experimental runs were conducted using the same recipe, which was derived using the approach discussed in the previous section but with different addition policies (Run 7 and 8 in Table 1): the conventional pseudo-living approach (PL, Run 7) and the optimal approach discussed in this work (defined "constant properties," CP, Run 8) and based on model-predicted flowrates $\hat{q}_{I_2}$, $\hat{q}_{DTA}$, and $\hat{q}_{DO}$. In the latter case, an initial APS shot equal to the 50% of the predicted total initiator amount was used to make the reaction time reasonably short. The results of these experiments are compared with the model predictions in Figure 7.

The number average molecular weight (Figure 7a) was continuously increasing with conversion in the PL case, as expected, while it remains practically constant all along the reaction using the designed continuous feed flowrates. Indeed, the implementation of optimal feed rates affects the polymerization mechanism, which is no longer pseudo-living. This is due to the different chain formation dynamics: in the PL case, the number of chains is mainly determined by the initial DTA shot, leading to a monotonic increase of M_n with conversion,

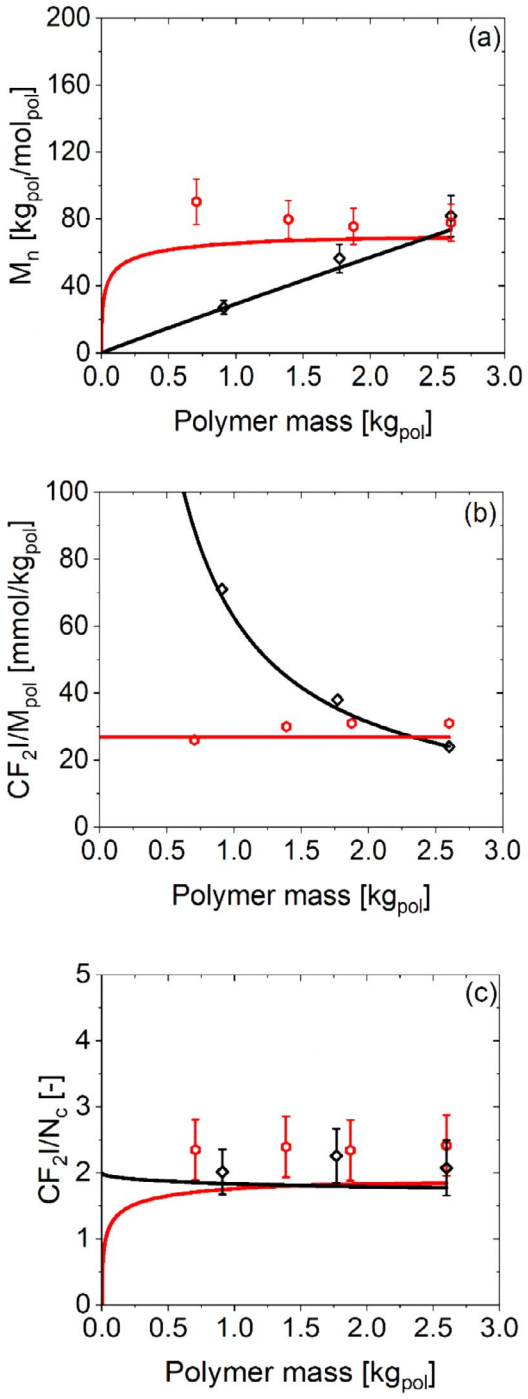

FIGURE 7 | (a) Number average molecular weight, (b) CF_2I chain end groups per mass of polymer, (c) CF_2I chain end groups per chain as a function of produced polymer mass. Experimental data: pseudo-living reaction = black symbols; constant properties = red symbols. Model predictions: continuous curves, black for pseudo-living and red for constant properties.

whereas under continuous feed conditions the constant availability of the chain transfer agent allows new chains to be steadily generated, proportional to the conversion, resulting in a constant M_n and the loss of pseudo-living character. Notably, the target value is quickly approached from the beginning in the latter case, despite the initial APS shot implemented to speed up the reaction. The homogeneity of the molecular weight is even clearer after looking at the experimental molecular weight distributions (MWD) reported in Figure S3a,b for the two cases. Apart from the increase of area below the peaks due to the conversion increase, the distributions remain in the same position in the CP case, while they shift along the horizontal axis in the PL case.

The completely different behavior of the average properties in the two cases is even more visible in Figure 7b, where the amount of iodinated chain end groups per mass of polymer is shown as a function of conversion. Even though the final values differ in the two cases because of the different incorporation efficiency, the much more homogeneous behavior established in the CP case is quite clear, both in terms of experimental data and model predictions. This marked homogeneity in the content of iodinated chain end groups per mass of polymer is directly linked to the continuous addition of DTA proportional to the conversion profile (cf. Section 6 of Supporting Information). As a result, its incorporation remains consistently aligned with polymer formation. In contrast, the evolution of M_n is influenced by the development of the number of chains, which is inherently affected by the initial APS shot.

Quite surprisingly, the number of iodinated end groups per chain reported in Figure 7c are instead quite similar but this is only due to a fortuitous compensation. As a matter of fact, the number of iodinated end groups per chain can be expressed as:

$$\frac{N_{CF_2I}}{N_c} = \frac{N_{CF_2I}}{N_{M_p}} \frac{N_{M_p}}{N_c} = \frac{N_{CF_2I}}{N_{M_p}} M_n \tag{26}$$

Accordingly, the increasing molecular weight on one side and the decreasing iodine content on the other make their product almost constant, even though the polymer remains heterogeneous in terms of chain lengths.

6 | Conclusions

The terpolymerization of vinylidene fluoride (VDF), hexafluoropropylene (HFP), and tetrafluoroethylene (TFE) has been carried out in the presence of two significant compounds, in addition to the thermal initiator: a degenerative transfer agent, as a perfluorinated di-iodinated species, and a cross-linking agent, i.e., a perfluorinated diolefin. The combination of these additives characterizes branching and pseudo-living polymerization technology, a technique that facilitates the design and optimization of the iodinated chain-end group density per polymer chain, a crucial parameter for subsequent curing processes.

In this study, we established a simplified model enabling the design of emulsion polymerization recipes ensuring the achievement of target values for number-average molecular weight, number of iodine end groups and branching points, as the properties affecting the most the polymer quality in this case, as well as their consistency along the reaction. The model was calibrated by fitting three sets of experimental data, through an optimization procedure aimed at determining the

unknown kinetic constants. The contribution of the degenerative transfer agent was considered based on existing literature and prior research. Particular attention was given to the formation of tetrafunctional branching points, resulting from diolefin reactivity.

Upon model calibration and validation, an analytical formulation was developed to estimate an optimal recipe and addition strategy for initiator, DTA and DO. The primary objective of the model is to ensure the highest homogeneity of the polymer in relation to the target properties from the earliest stages of the polymerization process. According to the model, this strategy leads to limited control over the reaction time, often resulting in an excessively prolonged polymerization process. From a practical perspective, the reaction kinetics can be managed by introducing a small initial dose of initiator, which accelerates the system, preventing prolonged phases with low conversion rates.

This approach results in a trade-off between product homogeneity and productivity demands. Still, by adding 50% of the planned initiator amount at the beginning, a heterogeneity of 9% only was achieved.

Finally, a polymer with desired target average properties has been selected and produced experimentally following the addition policy proposed by the model. The model predictions were found to align closely with experimental results in terms of M_n and chain end groups.

Additionally, a comparison was made with a pseudo-living process, using the same overall additive content. While the polymer average quality at the end of the process was very similar as that obtained with the continuous additive feeding as predicted by this model, the homogeneity could be preserved from the early stages of the polymerization. This benefit is particularly relevant in practical scenarios, such as when production lines must be shut down due to technical issues or safety concerns, ensuring that the product is already at the desired specifications and can be extracted, stored, and used without waste.

Nomenclature

APS	ammonium persulfate
BP	branching points
BR	bridges
C	chains
(CF_2CH_3)	CH_2CH_3 end groups
(CF_2H)	CF_2H end groups
(CF_2I)	CF_2I end groups
(CH_2OH)	CH_2OH end groups
CP	constant properties
DO	diolefin
DP_n	number average degree of polymerization
DTA	degenerative transfer agent
f	radical efficiency from initiation
GPC	gel permeation chromatography
H	Henry constant of the monomeric mixture
HFP	hexafluoropropylene
H_i	Henry constant of i-th monomer
k_{bb}	backbiting reaction rate constant
k_d	initiator decomposition rate constant
k_{des}	desorption rate constant
$k_{ex,1}$	degenerative transfer reaction rate constant
k_{fm}	chain transfer to monomer rate constant
k_{fp}	chain transfer to polymer rate constant
k_p	monomer propagation rate constant
k_p^{DO}	diolefin propagation rate constant
k_p^{PDB}	addition to pendant double bond rate constant
k_p^{TDB}	addition to terminal double bond rate constant
k_{td}	termination by disproportionation rate constant
M	monomer concentration
M_n	number average molecular weight
M_{pol}	mass of polymer
MWD	molecular weight distribution
MW_M	monomer mixture molecular weight
N_x	number of moles of species x
P	pressure
PDB	pendant double bond end group
PL	pseudo-living
$\hat{q}_x$	molar specific flowrate of species x
$\mathcal{R}_{M\,pol}$	polymerization rate
$\mathcal{R}_x$	kinetic rate of chemical event involving species x
T	temperature
t	time
TDB	terminal double bond end group
TFE	tetrafluoroethylene
VDF	vinylidene fluoride
V_p	particle volume
y_x	ratio between the overall numbers of moles of species x and of polymerized monomer

Greek Letters

β_i	effective kinetic ratios
θ	active sites (radicals)
ρ_M	monomer mixture density
ρ_{pol}	polymer density

Author Contributions

Luca Fois: investigation, writing – original draft, software. **Daniela Bertani:** writing – review and editing, resources. **Matteo Fantoni:** funding acquisition, writing – review and editing. **Mattia Sponchioni:** supervision, project administration, writing – review and editing, funding acquisition. **Giuseppe Storti:** funding acquisition, supervision, writing – review and editing.

Acknowledgements

Open access publishing facilitated by Politecnico di Milano, as part of the Wiley - CRUI-CARE agreement.

Conflicts of Interest

L.F., D.B., M.F., M.S., and G.S. are inventors of the patent no. EP4556496A1, whose applicants are Solvay Specialty Polymers Italy S.p.A. and Politecnico di Milano.

Data Availability Statement

The data that support the findings of this study are available from the corresponding author upon reasonable request.

References

1. R. Dams and K. Hintzer, "Chapter 1: Industrial Aspects of Fluorinated Oligomers and Polymers," in *Fluorinated Polymers: Volume 2: Applications*, ed. B. Ameduri and H. Sawada (Royal Society of Chemistry, 2016), https://doi.org/10.1039/9781782629368-00001.

2. M. Apostolo, V. Arcella, G. Storti, and M. Morbidelli, "Kinetics of the Emulsion Polymerization of Vinylidene Fluoride and Hexafluoropropylene," *Macromolecules* 32 (1999): 989–1003, https://doi.org/10.1021/ma980683r.

3. P. Maccone, M. Apostolo, and G. Ajroldi, "Molecular Weight Distribution of Fluorinated Polymers With Long Chain Branching," *Macromolecules* 33 (2000): 1656–1663, https://doi.org/10.1021/ma990982w.

4. C. Boyer, P. Lacroix-Desmazes, J. J. Robin, and B. Boutevin, "Reverse Iodine Transfer Polymerization (RITP) of Methyl Methacrylate," *Macromolecules* 39 (2006): 4044–4053, https://doi.org/10.1021/ma052358r.

5. B. O'Shaughnessy and D. Vavylonis, "Dynamics of Living Polymers," *European Physical Journal E: Soft Matter* 12 (2003): 481–496, https://doi.org/10.1140/epje/e2004-00020-9.

6. C. Boyer, D. Valade, P. Lacroix-Desmazes, B. Ameduri, and B. Boutevin, "Kinetics of the Iodine Transfer Polymerization of Vinylidene Fluoride," *Journal of Polymer Science Part A: Polymer Chemistry* 44 (2006): 5763–5777, https://doi.org/10.1002/pola.21654.

7. F. Brandl, M. Drache, and S. Beuermann, "Kinetic Monte Carlo Simulation Based Detailed Understanding of the Transfer Processes in Semi-Batch Iodine Transfer Emulsion Polymerizations of Vinylidene Fluoride," *Polymers* 10, no. 9 (2018): 1008, https://doi.org/10.3390/polym10091008.

8. M. H. Stenzel and C. Barner-Kowollik, "The Living Dead: Common Misconceptions About Reversible Deactivation Radical Polymerization," *Materials Horizons* 3 (2016): 471–477, https://doi.org/10.1039/c6mh00265j.

9. F. K. Hansen and J. Ugelstad, "Particle Nucleation in Emulsion Polymerization. I. A Theory for Homogeneous Nucleation," *Journal of Polymer Science* 16 (1978): 1953–1979, https://doi.org/10.1002/pol.1978.170160814.

10. Y. Dong, "A Molecular Theory for Particle Nucleation: Primary Particle Formation in Emulsion Polymerization," *Journal of Colloid and Interface Science* 326 (2008): 354–359, https://doi.org/10.1016/j.jcis.2008.06.033.

11. Y. Dong and D. C. Sundberg, "Radical Entry in Emulsion Polymerization: Estimation of the Critical Length of Entry Radicals via a Simple Lattice Model," *Macromolecules* 35 (2002): 8185–8190, https://doi.org/10.1021/ma020220s.

12. M. J. Barandiaran, J. C. de la Cal, and J. M. Asua, "Emulsion Polymerization," in *Polymer Reaction Engineering*, ed. J. M. Asua (Wiley, 2007), https://doi.org/10.1002/9780470692134.ch6.

13. J. M. Asua and J. C. De La Cal, "Entry and Exit Rate Coefficients in Emulsion Polymerization of Styrene," *Journal of Applied Polymer Science* 42 (1991): 1869, https://doi.org/10.1002/app.1991.070420708.

14. Z. Song and G. W. Poehlein, "Kinetics of Emulsifier-Free Emulsion Polymerization of Styrene," *Journal of Polymer Science Part A: Polymer Chemistry* 28 (1990): 2359–2392, https://doi.org/10.1002/pola.1990.080280911.

15. M. Apostolo and M. Morbidelli, "Microstructure Control in the Emulsion Polymerization of Fluorinated Monomers," *Chimica e l'Industria* 79 (1997): 361.

16. M. Albano, E. Barchiesi, R. Biancardi, M. Dossi, G. Geniram, and P. Vaccarono, "Comprehensive Characterization of Chain End Groups of Vinylidene Fluoride Based Polymers," *Macromolecular Symposia* 324, no. 1 (2013): 41–48, https://doi.org/10.1002/masy.201200065.

17. C. Boyer, D. Valade, L. Sauguet, B. Ameduri, and B. Boutevin, "Iodine Transfer Polymerization (ITP) of Vinylidene Fluoride (VDF). Influence of the Defect of VDF Chaining on the Control of ITP," *Macromolecules* 38, no. 25 (2005): 10353–10362, https://doi.org/10.1021/ma051349f.

18. M. Pianca, E. Barchiesi, G. Esposto, and S. Radice, "End Groups in Fluoropolymers," *Journal of Fluorine Chemistry* 95 (1999): 71–84, https://doi.org/10.1016/S0022-1139(98)00304-2.

19. M. Okubo and T. Mori, "The Decomposition of Potassium Persulphate Used as Initiator in Emulsion Polymerization," *Makromolekulare Chemie, Macromolecular Symposia* 31 (1990): 143–156, https://doi.org/10.1002/masy.19900310112.

20. Z. Xie and A. E. Hamielec, "Modelling Free-Radical Copolymerization Kinetics-Evaluation of the Pseudo-Kinetic Rate Constant Method, 2. Molecular Weight Calculations for Copolymers With Long Chain Branching," *Macromolecular Theory and Simulations* 2 (1993): 455, https://doi.org/10.1002/mats.1993.040020312.

21. V. Arcella, G. Brinati, and M. Apostolo, "New High Performances Fluoroelastomers," *Chimica e l'Industria* 79 (1997): 345.

22. G. Storti, S. Carra, and G. Vita, "Kinetics of Multimonomer Emulsion Polymerization. The Pseudo-Homopolymerization Approach," *Journal of Applied Polymer Science* 37 (1989): 2443–2467, https://doi.org/10.1002/app.1989.070370901.

23. M. Nomura, H. Tobita, and K. Suzuki, "Emulsion Polymerization: Kinetic and Mechanistic Aspects," in *Advances in Polymer Science*, vol. 175, ed. M. Okubo (Springer, 2005), https://doi.org/10.1007/b100116.

24. M. Apostolo, M. Albano, G. Storti, and M. Morbidelli, "Emulsion Polymerization of Vinylidene Fluoride and Hexafluoropropylene: Average Number of Active Chains Per Particle," *Macromolecular Symposia* 150 (2000): 65–71, https://doi.org/10.1002/1521-3900(200002)150:1<65::AID-MASY65>3.0.CO;2-V.

25. B. Ameduri, "From Vinylidene Fluoride (VDF) to the Applications of VDF-Containing Polymers and Copolymers: Recent Developments and Future Trends," *Chemical Reviews* 109 (2009): 6632–6686, https://doi.org/10.1021/cr800187m.

26. G. Zapsas, Y. Patil, Y. Gnanou, B. Ameduri, and N. Hadjichristidis, "Poly(Vinylidene Fluoride)-Based Complex Macromolecular Architectures: From Synthesis to Properties and Applications," *Progress in Polymer Science* 104 (2020): 101231, https://doi.org/10.1016/j.progpolymsci.2020.101231.

27. K. N. Thakore and H. M. Mehendale, "Difluoroethylene, 1,1," in *Encyclopedia of Toxicology*, 3rd ed., ed. P. Wexler (Academic Press, 2014), 149, https://doi.org/10.1016/B978-0-12-386454-3.00308-0.

28. J. Ugelstad, P. C. Mörk, and J. O. Aasen, "Kinetics of Emulsion Polymerization," *Journal of Polymer Science Part A: Polymer Chemistry* 5 (1967): 2281–2288, https://doi.org/10.1002/pol.1967.150050907.

29. J. Ugelstad and F. K. Hansen, "Kinetics and Mechanism of Emulsion Polymerization," *Rubber Chemistry and Technology* 49 (1976): 536–609, https://doi.org/10.5254/1.3534976.

30. B. Ameduri and B. Boutevin, "Copolymerization of Fluorinated Monomers: Recent Developments and Future Trends," *Journal of Fluorine Chemistry* 104 (2000): 53–62, https://doi.org/10.1016/S0022-1139(00)00227-X.

31. E. Mavroudakis, D. Cuccato, M. Dossi, G. Comino, and D. Moscatelli, "Quantum Chemistry Investigation of Fluorinated Polymer Systems of Industrial Interest," *Journal of Physical Chemistry. A* 118 (2014): 238–247, https://doi.org/10.1021/jp409384g.

32. B. Hanamirian, A. Agostini, I. Chaduc, et al., "Kinetic Investigation of the Emulsion Polymerization of Vinylidene Fluoride," *Macromolecular Reaction Engineering* 19 (2025): 19, https://doi.org/10.1002/mren.202400023.

33. J. M. Prausnitz, R. N. Lichtenthaler, and E. Gomes de Azevedo, *Molecular Thermodynamics of Fluid-Phase Equilibria*, 3rd ed. (Prentice Hall International Series in the Physical and Chemical Engineering Sciences, 1999).

34. C. Costa, A. L. Alberton, A. F. Santos, et al., "Kinetic Parameters of the Initiator Decomposition in Microwave and in Conventional Batch Reactors—KPS and V50-Case Studies," *Macromolecular Reaction Engineering* 9 (2015): 366–373, https://doi.org/10.1002/mren.201500013.

35. M. Apostolo, V. Arcella, G. Storti, and M. Morbidelli, "Free Radical Controlled Polymerization of Fluorinated Copolymers Produced in Microemulsion," *Macromolecules* 35 (2002): 6154–6166, https://doi.org/10.1021/ma0119575.

36. M. Howe-Grant, *Fluorine Chemistry: A Comprehensive Treatment* (Wiley, 1995).

Supporting Information

Additional supporting information can be found online in the Supporting Information section. **Table S1:** Mark-Houwink parameters, M_0 and β parameters. **Table S2:** Kinetic rate constants and reactivity ratios. **Figure S1:** Smith-Ewart (SE) plot of the average number of radicals per particle as a function of α' at different values of m. Blue, green, violet and orange curves represent SE plot for m equal to 0, 10^{-1}, 1 and 10, respectively. Black rhombs, circles and stars represent the experimental data at different conversion values for runs 1, 2, and 3 reported in Table 1, respectively. **Table S3:** Average number of radicals per particle, at different conversion for run 1,2, and 3. **Table S4:** Material balances with time, t, as evolutionary variable. **Table S5:** Definition of the effective kinetic ratios. **Table S6:** Physicochemical model parameters. **Figure S2:** (a) CF_2H chain end groups per mass of polymer as a function of produced polymer mass. (b) CF_2CH_3 chain end groups per mass of polymer as a function of produced polymer mass. (c) CH_2OH chain end groups per mass of polymer as a function of produced polymer mass. Experimental data: run 4 = red circles, run 5 = black circles, run 6 = blue circles. Continuous curves: model results, same color as the corresponding experimental data. **Figure S3:** Experimental MWD at different conversion values (run 7, Table 1). (a) Constant Properties reaction: black = 25%, blue = 50%, orange = 75%, red = 100% conversion. (b) Pseudo-Living reaction: black = 30%, orange = 70%, red = 100%. (c) final distributions: red = CP, black = PL.